IEEE Access
Multidisciplinary ⋮ Rapid Review ⋮ Open Access Journal

Received May 20, 2022, accepted June 6, 2022, date of publication June 10, 2022, date of current version June 17, 2022.

Digital Object Identifier 10.1109/ACCESS.2022.3182120

Evaluation of Beamsteering Performance in MultiuserMIMO Unmanned Aerial Base Stations Networks

GERMAN CASTELLANOS[1,3], ACHIEL COLPAERT[2], MARGOT DERUYCK[1], (Member, IEEE), EMMERIC TANGHE[1], EVGENII VINOGRADOV[2], LUC MARTENS[1], (Member, IEEE), SOFIE POLLIN[2], AND WOUT JOSEPH[1], (Senior Member, IEEE)

[1]Department of Information Technology, IMEC, Ghent University, 9052 Ghent, Belgium
[2]Department of Electrical Engineering, KU Leuven, 3000 Leuven, Belgium
[3]Department of Electronics Engineering, Colombian School of Engineering, Bogota 111166, Colombia

Corresponding author: German Castellanos (german.castellanos@ugent.be)

This work was supported by the Research Foundation Flanders (FWO) under Project S003817N and Project G098020N. The work of German Castellanos was supported in part by the Colfuturo (Fundacion para el Futuro de Colombia); and in part by the Colombian School of Engineering Julio Garavito, Doctoral Scholarship Colfuturo, under Grant PCB 2018. The work of Margot Deruyck was supported by the Research Foundation Flanders (FWO-V) under Reference 12Z5621N.

ABSTRACT Future wireless communication networks can benefit from Unmanned Aerial Base Stations (UABSs) to provide enhanced capacity to ground users (GU) in large and remote locations. Connecting UABSs to the terrestrial network presents several challenges, such as the limited gain traditional antennas need to maintain suitable wireless links between the core network, UABS, and GU. A convenient solution is to use MaMIMO (Massive Multiple Input Multiple Output) since it improves spectral and energy efficiency, thus providing high data rates while reducing power consumption. This paper proposes a Multiuser MIMO (MuMIMO) model for UABS aided networks to increase service range and served capacity. It uses hybrid beamforming and beamsteering on Terrestrial Base Stations (TBSs) and UABSs to grant access to mobile GU in a bicycle race scenario. Results show that using the mobile operators' locations will benefit the backhaul network's performance by duplicating the capacity compared to using a private operator. Furthermore, user coverage increases by 400% if MuMIMO is used, compared to a single beam MaMIMO network. The proposed scenario could achieve a channel efficiency of 6.5 bit/s/Hz in the access network and 8.6 bit/s/Hz in the backhaul network. Finally, the average UABS transmitted power is reduced by 2/3, increasing the number of used beams.

INDEX TERMS Backhaul, beamforming, beamsteering, massive MIMO (MaMIMO), multiuser MIMO (MuMIMO), radio access network, unmanned aerial base station.

I. INTRODUCTION

Over the last few years, the use of a Base Station (BS) mounted on a drone or UAV (Unmanned Aerial Vehicle), i.e., an Unmanned Aerial Base Station (UABS), has gained popularity as a promising solution for wireless connectivity. A UABS provides fast deployable connectivity and support for crowded or fast movable scenarios that require a vast bandwidth for a short period [1]–[3]. To connect a UABS to the core network, several design aspects need to be studied, such as the position of the UABS and the allocation of access and backhaul radio resources under channel constraints for highly mobile vehicles [4]–[6].

However, several problems need to be addressed when deploying UAVs in existing cellular networks. First of all, due to the nature of existing cellular networks, aerial users are being served by side-lobes since those are mainly designed to serve ground users. Next, interference levels rise both in the uplink (UL) and downlink (DL) due to Line-of-Sight (LOS) links of several terrestrial BS (TBS). Furthermore, more handovers occur when moving at high altitudes due to fragmented BS assignments [7], [8]. In addition, long-range coverage is diminished by the usage of omnidirectional antennas that increase the path loss, reducing the capacity of

The associate editor coordinating the review of this manuscript and approving it for publication was Zhen Gao.

the aerial network. Previous work proposed some solutions to mitigate the effects like optimising the UAV altitude, using more directive transmission, or optimising path planning for the UAV [4]–[6]. The research community is actively trying to address these concerns. A promising enabling technology for UABSs is Massive Multiple Input Multiple Output (MaMIMO) due to its scalability and potential to deliver high and stable throughputs. In a MaMIMO cellular system, base stations are equipped with many antennas simultaneously serving multiple single-antenna terminals. By using beamforming, the power is focused into a small region of space, thus reducing interference and improving energy efficiency [9], [10]. Enabling digital beamforming leads to the use of Spatial Duplexing Multiple Access (SDMA) and Multi-user MIMO (MuMIMO). Due to this unique set of features, MaMIMO and MuMIMO attracted significant attention from the wireless and UAV communities, [7], [10]–[15] with the limited attention paid to backhaul links [16], [17].

In our previous work [18], the UABS is connected to the Core Network (CN) using a facility in the supported area centre. A facility was composed of a crane with a high antenna connected to the CN and a truck that stores the UABS for future service. However, these fast deployable facilities raise several connectivity challenges for larger areas. As the UAV's battery lifetime increases, the UABS can travel over a more considerable distance; hence a higher communication range of the backhaul (BH) network is required. Considering TBS and using them to connect UABS will benefit the connectivity of the BH link. Using the sub-6 GHz band for backhaul connection will require a very high spectrum efficiency to achieve significant bit rates due to the limited bandwidth available in this band. As a result, the main challenge here is to optimise the channel efficiency of the backhaul part through the optimal placement of UABS and the maximisation of the antenna gains.

Using technologies like Massive MIMO (MaMIMO) in both the access and backhaul links for UABS will provide several advantages. By using beamforming with 256-antenna elements, the antenna gain could increase up to 24 dB, increasing the UABS connectivity range up to 8 times, thus extending the coverage of UABS-aided networks. In addition, the capacity will be increased too because, for higher antenna gains, higher SNR values at the receiver will be found, resulting in better Modulation and Coding Schemes (MCS) that support higher bit rates [19].

A. CONTRIBUTIONS

We consider a UABS-aided cellular network, where MuMIMO techniques are used at the access (UABS - user) and backhaul links (TBS - UABS). UABSs are mobile so that the network can be dynamically densified as it is envisioned for future beyond-5G and 6G networks. To the best of the authors' knowledge, MuMIMO evaluation on long-range UABS-aided networks, accounting for the access and BH network in realistic scenarios, has not been done yet.

The major contribution of this work is the performance evaluation of the beamforming for MuMIMO with movable equipment mounted on UABS. To this end, we upgrade the capacity-based tool from [18] to include realistic users' mobility and MuMIMO physical layer capabilities through the usage of MaMIMO technology. The simulator takes into account several real factors such as actual 3D map, semi-deterministic channel models, ground users' movable locations and their traffic demands, the legal beam power limitation, realistic location and parameters of terrestrial infrastructure, and drone performance; to optimally allocate UABS and ground users under realistic constraints. Using our simulator, we answer the following questions:

- Is the UABS range extended by using MuMIMO?
- Is the capacity of the UABS-aided network increased by using MuMIMO?
- Will mm-Waves outperform sub 6GHz bands?

B. PAPER ORGANISATION

This paper is organised as follows. Section II-B describes the related work reviewing the use of beamforming in UABS networks. Section III-G presents the network architecture and defines the characteristics of the considered MuMIMO technology. In Section IV-C, we describe the methodology with particular attention paid to the scenario definition, the simulation tool, and the evaluation parameters used in this work. Section V-D2 discusses the results and, finally, in Section VI the paper is concluded, and the directions of the future work are given.

II. BEAMFORMING IN UABS NETWORKS

This section describes the recent works in UABS networks and beamforming technology that can support vast bandwidths on beyond 5G networks (B5G).

A. UNMANNED AERIAL BASE STATIONS

Several reviews and tutorials [2], [20]–[22] have described the benefits of using UABSs in 5G networks. Lin *et al.* [22] present a review of the cellular communications challenges for UAVs, such as the aerial channel and the antenna patterns for 3D communications. However, their approach only evaluates 8×1 antenna arrays, and vertical down-tilted is not compensated. Mozaffari *et al.* [2], [21], [23] introduced the concept of a 3D wireless network. They provide the mathematical background for the user-UAV association in this type of network and discuss the importance of beamforming to maximise the spectral efficiency of the network. They propose an antenna array based on multiple drones and beam-steering capabilities through the location and spacing of the drones.

In addition, our work [20] offers a holistic overview of 3D wireless communication networks. We describe channel models relevant for simulation-based works and provide guidelines on their appropriate use. Additionally, we summarise state of the art related to UAVs as aerial users and

UAVs as UABS. The content of [20] is based on analytical, simulation, and measurement-based publications.

In [24], [25] Xiao, *et al.* present a review of the scenarios and challenges for UAV mmWave communications with beamforming capabilities. It covers the problem of the antenna misalignment in the backbone link for UABS, which reduced the antenna gain. Results show that for Hybrid beamforming (HBF) with SDMA, the achievable channel efficiency could be higher than 16 bit/s/Hz for a Signal to Noise Ratio (SNR) of 30 dB. Our previous work [5] compares the coverage of existing cellular networks in sub-6 GHz (1.8 GHz) to upcoming 5G mmWave (38 GHz) frequencies. Through semi-deterministic simulations, we show that UAVs flying at an altitude just above rooftop level have perfect coverage. On the other hand, UAVs operating at more significant altitudes suffer from large interference levels, resulting in UAVs not having any coverage at high altitudes. To tackle this problem, we show that using more directive links like beamforming in the mmWave spectrum will essentially solve these issues since directive transmission reduces the interference towards other flying equipment. Previously in [7], we concluded that mmWave beamforming could also provide a solution to the existing handover problems at significant altitudes due to fragmented assignment behaviour in existing networks.

B. MASSIVE MIMO BEAMFORMING AND BEAM MANAGEMENT ON UABS

Several authors are studying the advantages of using beamforming for UABSs. These studies can be divided into two groups based on the considered link type: (i) in the backhaul (between the UABS and the core network) and (ii) in the access network (between the UABS and the ground users).

First, we discuss the studies related to backhaul connectivity. In [26], the authors propose an algorithm that performs 3D tracking of the pencil beams connected to UAV. The algorithm predicts the angular speed and determines the direction of future frame transmissions. The authors of [27] developed an optimised beam stabilisation algorithm suitable for a relatively slight misalignment of unstable beams. In [28], a beamforming model is used for UAVs serving as User Equipment (UE) to maximise the Up-Link (UL) throughput while minimising the interference between traditional terrestrial and the UAV users. The results show that the capacity can be up to five times higher when using beamforming than an omnidirectional antenna system. The authors of [15] discuss the benefits of a multi-beam UL in a UAV to reduce the interference of ground BS and maximise the UL sum rate by using the BH as a link to establish a cooperative environment between ground BS. In [29], the authors explore the problems that arise from pilot contamination in MaMIMO for aerial users and propose a decontamination algorithm to minimise the channel misalignment for the UAV and ground BS.

Second, we discuss the studies considering beamforming in the access network. The authors of [30] introduce Beam Division Multiple Access (BDMA) to provide multiple access to ground users from aerial BSs in mmWave frequencies. However, they have found that the number of beams is limited for ultra-dense networks, restraining the network's performance. Next, Halvarsson *et al.* in [19], [31] present the results of testbeds for beamforming management in the 3.5 GHz, demonstrating bandwidth efficiency of 8.75 bit/s/Hz for LoS links and 2.5 bit/s/Hz in NLoS links for the 3.5 GHz band.

Finally, recent works have focused on the advantages of combining the access and backhaul network under the same network. This technology is called In-band integrated Access and Backhaul (IAB) systems. It explores the advantages of multi hoping to extend the ranges and capacity of the backhaul to the cost of additional overheads, multi-link backhaul management, and complex interference management protocols. [16], [17], [32]

Although several authors have researched the benefits of MuMIMO beamforming, in state of the art, there is no joint allocation mechanism for access and BH links using beamforming and beamsteering. In the following section, we propose a network architecture with an allocation mechanism to serve ground users with MuMIMO in UABS.

TABLE 1. Summary of the system model notation.

Notation	Definition
A_g	UPR Antenna Gain
AF	Antenna Array Factor
A_{min}	Antenna Minimum Gain
EG	Antenna Element Gain
EG_{max}	Antenna Element Maximum Directional Gain
θ	Elevation Angle of interest
θ'	Elevation Angle of Steered Beam
ϕ	Azimuth Angle of interest
ϕ'	Azimuth Angle of Steered Beam
M_g	Number of panels on the columns (x)
N_g	Number of panels on the rows (y)
β_x	Progressive Phased arrays (x)
β_y	Progressive Phased arrays (y)
I_i	Excitation Amplitude of element i
P	Total network power consumption
$P_{A,n}$	Power consumption of Access network for UABS n
$P_{BH,n}$	Power consumption of Backhaul network for UABS n
P_{DSP}	Power of the Digital Signal Processor (DSP)
P_{trans}	Power of the Transmitter
P_T	Radiated Power
η	Power amplifier efficiency
P_{Beam}	Power per beam
B_{used}	Used beams per antenna

III. NETWORK ARCHITECTURE FOR UABS

The following section describes in detail the network architecture for UABS. First, the access and BH network are described, then the details of the antenna and channel models are depicted, and finally, the parameter of the drones are presented. Details of the notations of these models can be found in Table 1.

A. RADIO ACCESS AND BH NETWORKS ARCHITECTURE

We consider a UABS network to provide wireless communication to ground users with video traffic requirements under

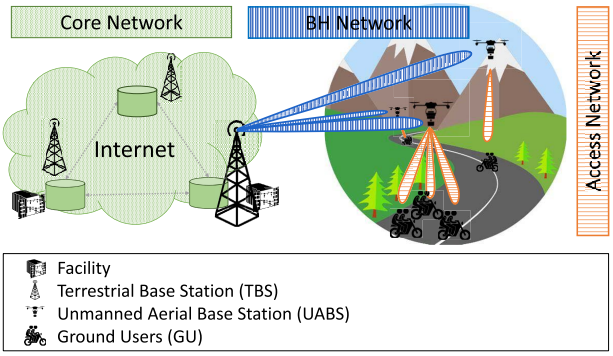

FIGURE 1. Network architecture for UABS with for MuMIMO capabilities.

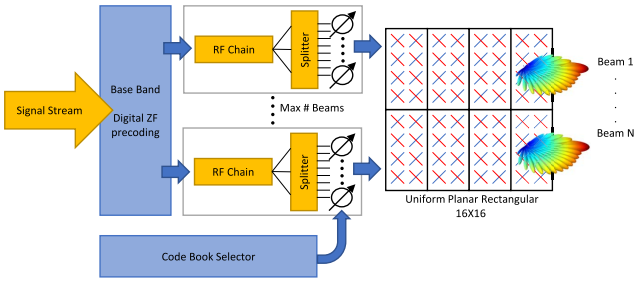

FIGURE 2. Multi-user MIMO Beamforming model used with code-book selector for multiple beams.

mobile conditions. The network architecture is shown in Fig. 1. It consists of the access network that allows ground users to be served by aerial Base Stations and the backhaul network to enable UABS to be connected to the core network through terrestrial Base Stations. This architecture is based on our previous work [18], [33], [34] with two main improvements. First, the system model considers now the dynamic allocation of ground users based on realistic movements (differing from the fixed random location). Secondly, we include a complete physical model for the Massive MIMO and Multi-user MIMO, including the 3D geometry of the UAV system that consists of the Uniform Planar Rectangular (UPR) array antennas.

The Radio Access Network (RAN) provides access to the mobile ground users (GU) through the UABSs, as shown by the orange links (horizontal patterns) in Fig. 1. On the other hand, the BH network (blue links (vertical patterns)) connects each UABS with the core network in Fig. 1). As shown in Fig. 1, the BH network consists of terrestrial base stations (TBS). The UABS typically connects to the TBS, from which it experiences the lowest path loss. We assume intra-cell handover and frequency management are internally done on the TBS, and details of the allocation procedures will be described in the methodology section.

B. MULTI-USER MIMO SYSTEM

In order to serve multi-user using MIMO technology, MuMIMO beamforming has been implemented. Fig 2 illustrates the MuMIMO hybrid beamforming model used to serve multiple beams simultaneously, based on the BDMA method in [30], [35], where diverse beams are steered based on a specific code for each beam set. The signal streams for each beam are Regularized Zero Force (RZF) precoded in the baseband and further transmitted to the RF chains. RZF precoding is selected to reduce the intra-beam interference based on the knowledge of the Channel State Information (CSI) [36]–[39]. Each RF chain is in charge of each beam, so the number of RF chains is determined by the maximum number of supported beams, in our case, 8 beams [40]. Then, the phase shifters are controlled by a code-book selector (CBS) in charge of steering to the desired location of each beam based on pilots and CSI values.

Here, the hybrid beamforming provides digital precoding to minimise the intra-beam interference based on the RZF, while the analogue precoding, controlled by the CBS, is in charge of the steering process. The CBS controls the division of the total number of antennas of the antenna array into sub-arrays with an equal number of antennas to maintain equal maximum gain among the different beams; in this way, the same beamforming model works for 1, 2, 4 or 8 beams as controlled by the CBS [41], [42]. We assume that our CBS plans a jointly coordinated allocation method among the UABS to reduce interference by selecting the appropriate code-book for each beam in a coordinated fashion [44]. Finally, based on previous simulations obtained in our tool, we added an Interference MuMIMO Margin of 2 dB to our link budget to account for other interference values not accounted for [43].

C. UNIFORM PLANAR RECTANGULAR ARRAY ANTENNAS

The antennas of the TBS and on-board of the UABS are described here. Each TBS is provided with a 3-sector antenna to support 360-degree coverage. Each sector has a Uniform Planar Rectangular array (UPR). The UPR contains an $M_g * N_g$ Cross-polarised panel. M_g represents the number of panels on the columns (x), while N_g is the number of panels on the rows (y). We will evaluate the performance of the 8×8, 16×16, and 32×8 array sizes for the BH link. As described in [44], [45], these antenna panels are uniformly spaced in both directions and dual-polarised. The 3D radiation pattern of each antenna is constructed based on the array's gain using spherical angles on the Cartesian coordinates. The antenna gain A_g is determined by (1) [44], [45]:

$$A_g(\theta, \phi)[dB] = AF(\theta, \phi) + EG(\theta, \phi) \tag{1}$$

where AF is the antenna array factor in dB as a function of the elevation θ and the azimuth ϕ. EG in dB, is the element gain of the antenna and defined as follows:

$$EG(\theta, \phi)[dB] = max(A''(\theta, \phi = 0°) + A''(\theta = 90°, \phi), A_{min}) + EG_{max} \tag{2}$$

$$A''(\theta, \phi = 0°)[dB] = max\left(12\left(\frac{\theta - 90°}{\theta_{3dB}}\right)^2, A_{min}\right) \tag{3}$$

$$A''(\theta = 90°, \phi)[dB] = max\left(12\left(\frac{\phi}{\theta_{3dB}}\right)^2, A_{min}\right) \tag{4}$$

where $A''(\theta, \phi = 0°)$ and $A''(\theta = 90°, \phi)$ are the vertical and horizontal cut of the radiation power patterns in dB, $\theta \in [-90°, +90°]$ while $\phi \in [-180°, 180°]$, θ_{3dB} is the aperture angle of the antenna and is set to 65°, A_{min} is set to -30 dB and EG_{max} is the maximum directional gain of the antenna element.

$$AF[dB] = 10log_{10}\left(|AF_{x1} \cdot AF_{1y}|\right) \tag{5}$$

$$AF_{x1} = \sum_{m=1}^{M_g}\left(I_{m1}e^{j(m-1)(kd_x sin\theta' cos\phi' + \beta_x)}\right) \tag{6}$$

$$AF_{1y} = \sum_{n=1}^{N_g}\left(I_{1n}e^{j(n-1)(kd_y sin\theta' sin\phi' + \beta_y)}\right) \tag{7}$$

$$\beta_x = kd_x sin\theta_0 cos\phi_0 \tag{8}$$

$$\beta_y = kd_y sin\theta_0 sin\phi_0 \tag{9}$$

The Array Factor AF in dB is the logarithmic function of the product of the array factor in the x-axis (AF_{x1}) and the y-axis (AF_{1y}). $I_{m1} = I_{1n} = I_0$ is the excitation amplitude of the elements, and for a UPR, they are constant. β_x and β_y are the progressive phases of the array. Denoted as d, is the distance between the radiation elements and is defined as $d = \lambda/2$ and $k = 2\pi/\lambda$. If the beams are steered, θ' and ϕ' will be pointed towards the direction of the desired steering determined by the code-book; otherwise, $\theta' = \theta$ and $\phi' = \phi$.

Multibeam forming is achieved by dividing the UPR into sub-arrays containing an equal number of antenna elements. As shown in Fig 2, a 16 × 16 antenna array is divided into 8 beams with 8 sub-arrays of 4×8 elements and equations (1) to (9) will be applied for each beam.

The UABS will carry a similar UPR antenna system for the access and backhaul networks. While the backhaul antenna array will be pointed towards the horizon, the access antenna array will be pointed downwards. We also assume that the placement of these antennas does not affect the flying capacities of the drone. However, this system will be limited in size for practical reasons, i.e., 0.68 × 0.68 m for the 16 × 16 elements and 0.34×0.34 m for the 8×8 elements. Larger antenna sizes for the sub-6 GHz band will be impractical on the UAV. Using 64 and 256 antennas leads to channel hardening in reducing the impact of small-scale fading and spatial correlation. This is because the collinearity of the channel matrix for these antenna sizes disappears for inter-user distances of 20 m and 10 m, respectively [46], [47]. A coordinate conversion for the angles needs to be implemented as the access antennas will be pointed downwards.

D. MISALIGNMENT MANAGEMENT

Due to the nature of the moving environment of the UABS, some assumptions are made regarding the misalignment problems. First, the digital beamforming uses a resolution of 1 degree in each axe, meaning that the code-book used to steer the beam in the UPR is a matrix of 130 by 130 phased signals. This also means that if the link angle (denoted by θ and ϕ) is in the middle of two possible digitally steered beams (denoted by θ' and ϕ'), the gain assigned to this link will be calculated according to equations (5) to (9). Second, we assume that pilots can beam track the locations of the movable equipment in each timestamp. Based on [7], [26], we assume a 3D beam-tracking reference model that estimates the angular speeds of the beams through a dynamic pilot insertion which can maintain 95% beamforming gain while increasing only 0.1% pilot overhead. This model also includes a fusion sensor that aids in long-range and fast-moving systems [48].

In addition, we assume that the weather conditions of the environment do not affect the ability of the UAV to maintain a stable beam and that the maximum angular speed of the movable nodes is smaller than the maximum shifting delay of the digital beams, which is around 10 ms [49].

TABLE 2. Link budget parameters for access and backhaul networks. [18], [33], [50], [51].

Parameters	Units	Access	BH	
		5G	Sub6GHz	mmWave
Frequency	GHz	2.6	3.5	61.5
Bandwidth	MHz	5	20	1000
Antenna Gain	dBi	8	6	8
Resource Blocks	-	20	100	5000
Used subcarriers	-	320	1200	60000
Total subcarriers	-	512	2048	116500
Max Tx Power	dBm	26	49	43
Fade Margin	dB	10	10	5
Noise Figure	dB	5	5	5
Shadowing Std	dB	6	8	8
Doppler Margin	dB	3	3	3
Interference	dB	2	2	2
User Height	m	1.5	-	-
CN Height	m	-	25	25

E. FREQUENCY AND CHANNEL MODELS

The following section describes the frequency and channel models used in the backhaul and access links. For this network, we propose a narrow bandwidth scenario. This means access and backhaul channels are limited, i.e. 5 MHz for access and 20 MHz for BH in sub-6 GHz bands.

1) BACKHAUL NETWORK

For the backhaul links, we evaluate two bands, the 3.5 GHz and the 60 GHz. First, we assess the 3.5 GHz band, which has the best compromise between coverage and capacity in line-of-sight (LoS) and non-line-of-sight (NLoS) environments, supporting the easy operation of the network. However, the limited offered spectrum, larger antennas, and the need for efficient interference management are significant disadvantages for this band [18], [52], [53]. Current 5G trials have shown up to 10.4 Gbps data rate peaks using 200 MHz bandwidth on this frequency, demonstrating this band's potential in fulfilling the backhaul requirements [54]. Second, we study the 60 GHz band for having massive available bandwidth

TABLE 3. Receiver Signal-to-Noise Ratio (SNR) for Modulation and Coding Scheme (MCS) for different technologies. [18], [33], [50], [51].

Access Network	BH Network	
5G	Sub-6 GHz	mmWave
(0.15)QPSK=-7.8	1/4QPSK=-6	
(0.88)QPSK=0.2	1/3QPSK=-1.5	
(1.48)16QAM=3	1/2QPSK=3	1/4BPSK=3.4
(2.41)16QAM=10.5	2/3QPSK=10.5	1/2BPSK=7.4
(2.73)64QAM=14	1/216QAM=14	1/2QPSK=15.4
(5.12)64QAM=19	2/316QAM=19	1/216QAM=17.5
(5.55)256QAM=23	1/264QAM=23	
(6.91)256QAM=29	2/364QAM=29	

that will overcome the high path losses of these frequencies. This band is also suitable for UABS applications because it has more than 9 GHz of unlicensed spectrum that could be easily used and deployed for diverse sports events or other infrequent situations. The channel model used for the backhaul link is the 3GPP TR 36.777 path loss model [55] defined for connectivity between TBS and aerial vehicles.

2) ACCESS NETWORK

Compared with the BH links, we only evaluate the 2.6 GHz band for the access link. We used a different frequency band for the access network to limit the interference between both networks. Like the 3.5 GHz band, the 2.6 GHz presents a good balance between coverage and capacity. This band also performs better in NLoS communications, which is very useful for the access network where ground users could be covered by buildings or inside of them. We assume a Time Division Duplexing (TDD) network for 5G technologies with 25% for DL and 75% for the UL in both links.

In addition, we selected Al-Hourani's Air2Ground path loss model for our access link [56], which was modelled based on ray tracing urban and suburban scenarios and tuned for our selected frequencies.

Shadowing fading has a substantial impact on the MIMO channel. We select the standard deviation for the shadowing fading based on the frequency and flying altitude of the UABS described in Table B-3 of the 3GPP TR 36.777 [55] and Table 7.4.1-1 of the 3GPP TR 138.901 [44] standards. These are based on Rayleigh distribution and have proven to provide a tangible impact on the fading channels for MIMO [9].

In addition, the LoS/NLoS calculation is realised by a Ray tracing where the obstruction is calculated based on the environment and the obstacles of the direct link between transmitter and receiver. We use the approach of [57] to realise this.

Finally, the radio link budget used for the proposed network is enclosed in Table 2, with detailed emphasis on the Receiver SNR for different Modulation and Coding Scheme (MCS) within diverse technologies (See Table 3) [50], [51].

F. UNMANNED AERIAL VEHICLES

Each UABS comprises BS equipment mounted in a long endurance Harris H4 HL hybrid quadcopter able to support nearly 3 hours of flight time. Its payload capacity and a wingspan of 2m are sufficient to carry a large antenna array. Details of the drone parameters used in our architecture are found in Table 4.[1]

TABLE 4. Drone parameters used in the simulation [18], [33], [58].

Parameter	Units	Value
Typical Payload	kg	3
Max Payload	kg	15
Typical Flight time	min	180
Max Speed	km/h	54
Wingspan	m	2.3

Also, if drone endurance is insufficient, we consider some facility locations with storage capabilities near the TBS for recharging operations, as shown in Fig. 1. These facilities, close to the initial TBS, can store up to 25 carriers with the possibility of switching and recharging the batteries of drones as they are depleting to keep all of them in the air. The location of the facilities is further studied in this paper based on the scenario selected.

G. POWER CONSUMPTION MODELLING

The total network power consumption $P(t)$ is the total power consumption of the wireless network, including the access and BH networks, at time t:

$$P(t) = \sum_{n=1}^{N} \left(P_{A,n}(t) + P_{BH,n}(t) \right) \tag{10}$$

where $P_{A,n}(t)$ and $P_{BH,n}(t)$ are the access and BH power consumption of each UAV-BS n during time slot t. If UAV-BS n is not active, $P_{a,n}^{(t)}$ and $P_{BH,n}^{(t)}$ are expressed as zero. The LTE power consumption models (in watt) for the access and BH networks for each UAV-BS n are based on [33] and [59]:

$$P_{A,n} = n_{sec} \left[P_{DSP} + A_g \left(P_{trans} + \frac{P_T}{\eta} \right) \right] \tag{11}$$

$$P_{BH,n} = P_{DSP} + A_g \left(P_{trans} + \frac{P_T}{\eta} \right) \tag{12}$$

where n_{sec} is the number of sectors of the access network, P_{DSP} is the Digital Signal Processor (DSP) power consumption in watts, the A_g is the MIMO gain of the transmitter, the P_{trans} is the power used by the transceiver, the P_T is the actual radiated power by the antenna and η is the power amplifier efficiency.

To evaluate the transmitted power per beam, the total transmitted power of the antenna is divided by the used beams as described in (13):

$$P_{Beam} = \frac{P_T}{B_{used}} \tag{13}$$

where P_{Beam} is the power of the evaluated beam in Watts, P_T is the transmitted power of the antenna in Watts, and B_{used} is the number of used beams of that particular link.

[1]Harris hybrid quadcopter: https://www.harrisaerial.com/carrier-h4-hybrid-drone/

Finally, the power needed by a UAV-BS for flying is considered constant; it does not vary with weather conditions or weight variances and allows to determine the service time of the specific UABS. i.e. the service time will be determined by the network power consumption. Once a UABS runs out of battery, a new UABS will fly to the position of the ageing UABS, and a seamless handover is applied.

IV. METHODOLOGY: NUMERICAL ANALYSIS AND SIMULATION MODELLING

The following section describes the Tour of Flanders scenario used for the numerical analysis and the java-based tool developed to perform the simulations.

A. SCENARIO DEFINITION

To make this work more tangible, we consider a real scenario of the Tour of Flanders, which is an annual cycling race on Flanders' cobblestone roads. It is one of the major cobbled classics in Flanders, Belgium. The cyclists cover a track of 267 km over both flat terrain and climb stretching from Antwerp to Oudenaarde.[2]

1) ARCHITECTURE

We design our scenario to match this cycling race's communication requirements and constraints realistically. The communication link is composed of a backhaul and an access link, where the BH link is between a TBS and the UABS following the cyclists overhead at an average speed of 45 km/h. The access link exists between the UABS and ground users represented by the motorbikes following the cyclists and filming the race from the ground. There is one motorbike cameraman designated for the leader of each participating team, resulting in a total of 25 ground users. Each cameraperson uploads a video stream with an average bit rate of 10 Mbps. We evaluate the scenario every 30 seconds, defined as a timestamp, for 756 timestamps over the whole race duration. The location of the cameraman's bike is determined by the average cyclist speed in each location using the Simulation of Urban Mobility (SUMO) tool[3] and the route map. The UABSs are deployed over the bikes at 80 m height, as suggested in [18], at random locations. Further, a proximity avoidance algorithm restricts the minimum distance between drones to 25 m to prevent collisions.

2) SCENARIOS

Next, we define three scenarios to evaluate the beam steering performance in the UABS network (see Table 5). Scenario 1: ''Single-beam digital beamforming'' considers a single UABS connected to the TBS to explore the digital beamforming capabilities of the BH, such as beamsteering connectivity, frequency, and size of antennas. The No-Beamsteering scenario is based on a 3-sector antenna in the TBS that point its main lobe to the North, Southeast, and Southwest, while the beam steered one follows the location of the UABS. The 5G access link will use omnidirectional antennas on both sides. Scenario 2: ''Multibeam beamforming in the BH network'' investigates the performance of Multi-User beamforming (MuBF) in the BH by modifying the maximum number of beams. Multiple UABS are introduced and are being served simultaneously. The access network still uses omnidirectional antennas. Finally, in Scenario 3: ''Multibeam beamforming in Access and BH networks'', the UABS is equipped with a URA enabling MuBF in the access network. The best configuration determined in Scenario 2 is used for the BH link, and the scenario is further explored by varying the number of beams in the access network. A short description of these scenarios is presented in Table 5.

TABLE 5. Scenarios used in the simulation: Omni: Omnidirectional antenna, BF: Beamforming, MuBF: Multiuser MIMO Beamforming.

Sce	Description	UABS	Access	BH
1	Single beamforming	1	Omni	BF
2	Multi-BF in BH	Multi	Omni	MuBF
3	Multi-BF (Access & BH)	Multi	MuBF	MuBF

3) GROUND INFRASTRUCTURE

The locations of the TBS are a critical aspect of the scenario's definition. The area considered covers 65 km from east to west and 55 km south to north, covering the whole race track. In this area, we use two placement strategies. The first one considers a grid-based private BS allocation, proposing a grid with equally distributed 1, 4, 16, and 64 private locations, as shown in Fig. 3a. The second approach considers the list of 2151 existing Terrestrial BSs from the operators in the Flanders region. The distribution of these BS locations is presented in Fig. 3b. In both figures, the route is depicted with the green dots for each timestamp in the race. The blue, red, purple, and orange markers in Fig. 3a. describe the locations of the grid-based 1, 4, 16, and 64, respectively, while the yellow stars in Fig. 3b. depict the actual locations of the BSs in Flanders.

To understand the impact of the different location strategies, Table 6 lists important distance parameters for each strategy; the last column presents the distance experienced by a drone to a TBS in the farther case. The last column represents the furthest distance from a TBS to a drone following the race. Using the second strategy, the furthest TBS is at a maximum distance of 3.5 km. On the other hand, within the 64 BS grid approach, the maximum experienced distance is doubled compared with the existing BS list approach. Still, it is a feasible solution since the deployment will not depend on an established operator but rather on a private network operator.

B. SIMULATION TOOL

We propose a Java-based simulation tool that comprises network planning capabilities for UABS considering the access

[2]Ronde van Vlaanderen - Elite Men: http://www.rondevanvlaanderen.be/en/rvv/elite-men

[3]Simulation of Urban Mobility (SUMO): https://www.eclipse.org/sumo/

TABLE 6. Terrestrial BS (TBS) location analysis (Distances in km).

TBS	Inter TBS distance	Average Drone-TBS distance	Maximum Drone-TBS distance
1	-	34.7	57.2
4	51.1	16.2	28.2
16	25.5	7.1	13.7
64	12.7	3.4	7.2
BS List	-	1.1	3.5

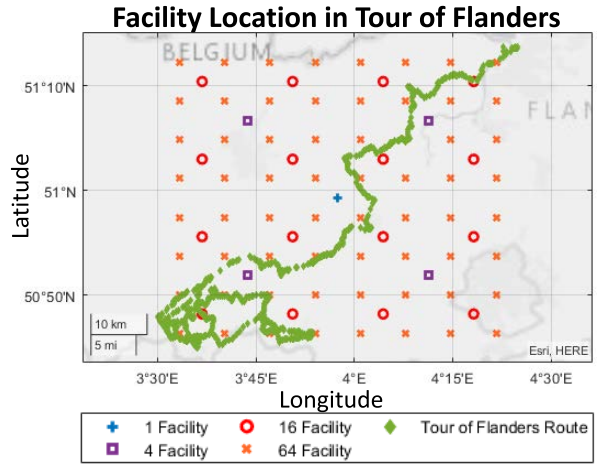

(a)

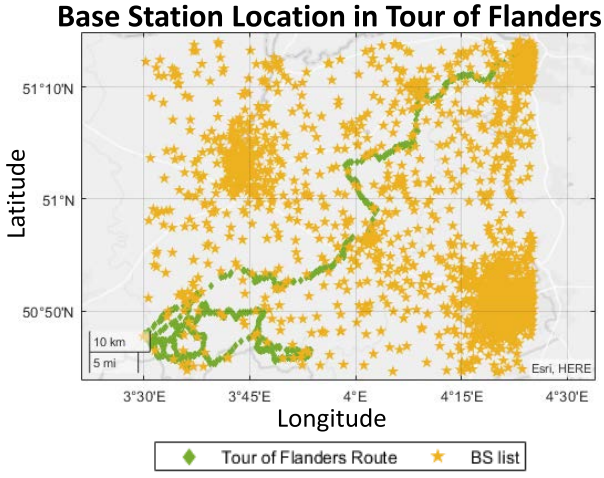

(b)

FIGURE 3. Terrestrial BS distribution a) Grid-based. b) Operator Base Station list.

and BH links. It is an extension of the capacity-based, energy-efficient simulation tool, which takes into consideration 3D realistic maps, semi-deterministic channel models and legal beam power limitations [18], [33], [60]. This version includes the creation of the MuMIMO digital beamforming calculation of the MIMO gain for 5G deployments. The UABSs are dynamically placed based on ground users' requirements and the network's restrictions within the proposed scenarios in the tool. The allocation procedures are done in a centralised way and are located in the facility entity. This assumption includes perfect knowledge of the location of UABSs, ground users,

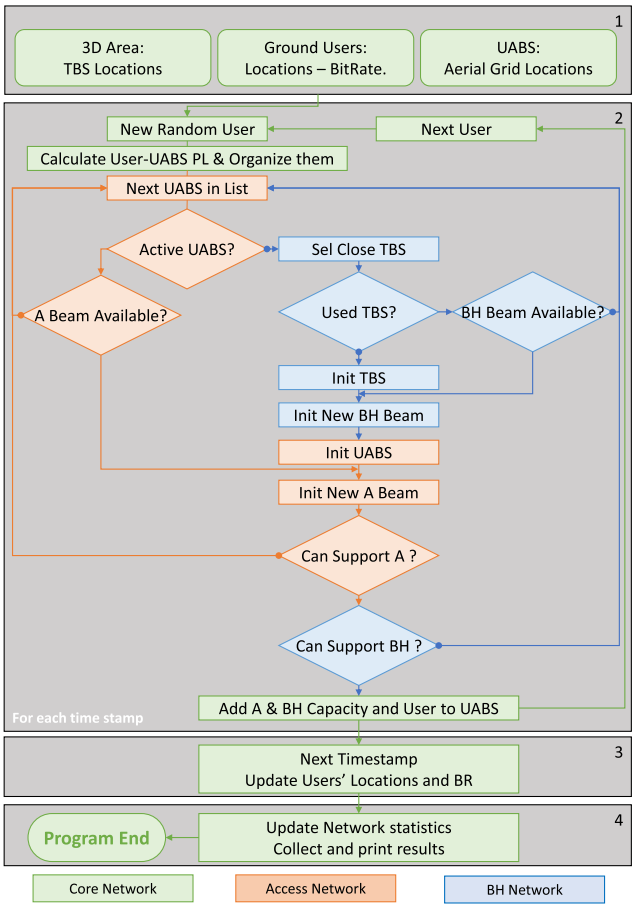

FIGURE 4. Flow diagram used in the Mu-MIMO evaluation.

and its traffic requirements. Moreover, the mobility aspect of the tool is achieved in a time stamp fashion, which is defined as a period in time of each evaluation of the network. Fig. 4, presents the flow diagram algorithm to perform the analysis of the MuMIMO. It is divided into four parts:

1) Initialises the simulation algorithm.
2) Describes the Access and BH allocation process.
3) Defines the mobile parameters implemented.
4) Collects the statistics for post-processing analysis.

1) PART 1: SIMULATION INITIALISATION

The algorithm starts by defining the three-dimensional locations of the considered area, as shown in Fig. 3. This includes the locations of the buildings in the area to evaluate whether a link is LoS or NLoS. Next, all the ground users' locations and traffic requirements are defined. Next, the possible locations list of the UABSs is created following the altitude and safety distance parameters described in the previous section. This information is used to create data for more than 6 hours of locations and requirements for all the network elements.

2) PART 2: ALLOCATION PROCEDURES

This part of the algorithm will be repeated for each timestamp of the simulation and is responsible for the design of the access network (orange steps) and the backhaul network

(blue steps). First, the algorithm will select a random user and calculate the path loss (PL) to each possible UABS location (green steps). Second, the algorithm will order the list of the possible UABSs according to this PL value by starting with the active UABSs and then the inactive ones. An active UABS is the one that has already a viable BH link and could support at least one ground user. On the other hand, an inactive UABS is the one that could have a possible BH nut no users have been assigned to it. The algorithm will now select the first UABS from this list (orange steps). Depending on whether the UABS is active, the tool will take the following actions:

1) If the UABS is not active, the most appropriate TBS needs to be determined (blue steps). The algorithm will select the closest TBS and identifies if it was already used. Again we have two options:
   - I The TBS is already in use: The algorithm will determine if some backhaul beams are still available. If this is the case, the initialisation of a new BH beam can start as follows:
     - i) The total transmitted power of the antenna is calculated.
     - ii) The azimuth and elevation angles of the UABS are calculated.
     - iii) The exact MIMO gain is calculated.
     - iv) The Path Loss is calculated. If this path loss is below the maximum allowable path loss, the UABS can be connected to this TBS.

     If no beams are available or the BH is not supported, the next UABS of the list is selected.
   - II The TBS is not in use: The algorithm initialises the TBS, and the initialisation of a new BH beam begins.
2) If the UABS is already active, we have to evaluate if there are available beams on the access network (orange steps):
   - I If no beams are available, the next UABS of the list is selected.
   - II If there are available beams, the UABS initialises a new beam in the access network following similar procedures to the one in the BH network.
   - III Then, an evaluation of the capacity is performed.
3) After the access and BH beams are initialised, the UABS proceeds to jointly assess if the capacity of both links could be served with the actual parameters by the following actions:
   - I Increase the antenna's input power ($P_{Antenna}$) until the link is served or the power reaches the maximum limit.
   - II If the maximum limit is reached in some of the access or the BH antenna, the input power is returned to the previous values, and the next UABS is evaluated.
   - III The SNR is used to determine the MCS. It is used with the requested bit rate to calculate the RB [18], [34] and add them to the aggregated BH link.
   - IV If both links could support the requested capacity, this is added to both links, and the user is allocated to that UABS.
4) Finally, an optimisation process of the other links is done to maximise the network's capacity. The allocation algorithm evaluates if UABS with one single user could transfer this user to the next UABS in the PL list. This is done by increasing the transmitted power, providing better MCS that reduces the number of required resource blocks in each link.

3) PART 3: MOBILITY

This part of the algorithm updates the location of the ground users based on the selected scenario and the UABS accordingly, preparing for the next timestamp. In addition, the list of active UABSs is evaluated, looking for UABSs that need battery replacement/recharging.

4) PART 4: POST-PROCESSING

In this final part, the algorithm collects the results and metrics of all the timestamps, users, and UABSs and logs them in CSV files for future post-processing and analysis.

C. SIMULATION METHODOLOGY

To achieve confident results in our simulation, we investigate the stability of the simulations. It is reached when the average value of the variables in a specific simulation has a deviation of $\pm$ 0.5 % of the average value over 100 simulations. This result is obtained with 40 simulations per scenario. Hence, for each simulation configuration, 40 independent simulations are executed.

For each scenario, a series of parameters are varied to evaluate the performance of each scenario. In scenario 1, we modified the beamsteering type (No beamsteering v.s beamsteering following the UAV), the number of Terrestrial BS, and the central frequency (3.5 GHz and 6 GHz). In scenarios 2 and 3, we modified the number of requested users and the maximum beams in the MuMIMO link. For the last scenarios, we evaluate the coverage and capacity of the network as explained in detail in Sec V-B and Sec V-C.

Finally, the whole bicycle race has 6 hours and 20 min (756 timestamps). Numerical results present the 95th percentile (p_{95}) over these 756 timestamps if not stated otherwise.

V. SIMULATION RESULTS AND DISCUSSION

The following Section provides insights into the three proposed scenarios and discusses the main findings. A general overview of scenarios is given in Table5.

A. SCENARIO 1: SINGLE BEAM DIGITAL BEAMFORMING

This scenario considers a single UABS. We evaluate the antenna and beam steering performance only in the BH network.

1) COVERAGE IN SCENARIO 1

Fig. 5 depicts the 95th percentile (p_{95}) showing that 100% connectivity is possible only for the beamsteering cases independent of the number of available TBS (continuous lines); however, if no beam steering is used (dashed lines), the connectivity drops to 87% for an 8×8 antenna (blue line) and 92% for a 16×16 antenna (yellow line) with only 1 TBS.

2) CAPACITY IN SCENARIO 1

Fig. 5b depicts the BH network resource block (RB) usage (p_{95}), where the number of resource blocks is inverse proportional to the number of available TBS. The more available TBS, the closer it is to the UABS, as seen in Table6, resulting in lower PL values. As a result, using the operators' TBS list, the use of RBs is four times fewer RBs compared to only one private TBS. Also, when using the beamsteering technique, 25% fewer RBs are used compared to no beamsteering. For the 16 and 64 private TBS, a reduction of 65% and 45% in the RB usage can be seen.

3) 60 GHz EVALUATION

We evaluate the performance of the 60 GHz frequency compared with the 3.5 GHz., as shown in Fig. 6. The 60 GHz band performs poorly compared with the 3.5 GHz and cannot provide 100% connectivity as described by the p_{95}, even when using a 16×16 antenna system and the operators' TBS list. The beamsteering technique outperforms the no beamsteering by more than three times (94% versus 25%), still not sufficient for 100% connectivity. This happens because the maximum antenna power in 3.5 GHz is 6 dB higher than 60 GHz. Moreover, the bandwidth is 50 times larger, raising the noise floor by 17 dB for 60 GHz, while the minimum SNR to achieve connection is 7 dB higher, leading to a difference of 30 dB for the minimum requirements for establishing the connection. In addition to the differences in the path loss due to the frequency, this leads to the poor performance of the 60 GHz band. To solve this problem, higher antenna power, improvements in the sensitivity of the MCSs, and better channelling for this band will improve the mmWave band's performance.

4) MULTI GROUND USERS' CONNECTIVITY

We include various ground users in the network to see the capacity in the single beam network with beamsteering and 16×16 antenna size. As explained in SectionIV-A, we increase the number of camerapeople motorbikes from 1 to 25. Results show that a single drone could support up to seven ground users in the best-case scenario (yellow line). This corresponds to the maximum capacity of a single BH link which adds up 72 Mbps (p_{95}) when using the best MCS, as shown in Fig. 7. For this case, the BH is the network's limitation since we assume no limit in the access network capacity. Also, the operators' TBS list usage doubles the served capacity for the multi-user scenario

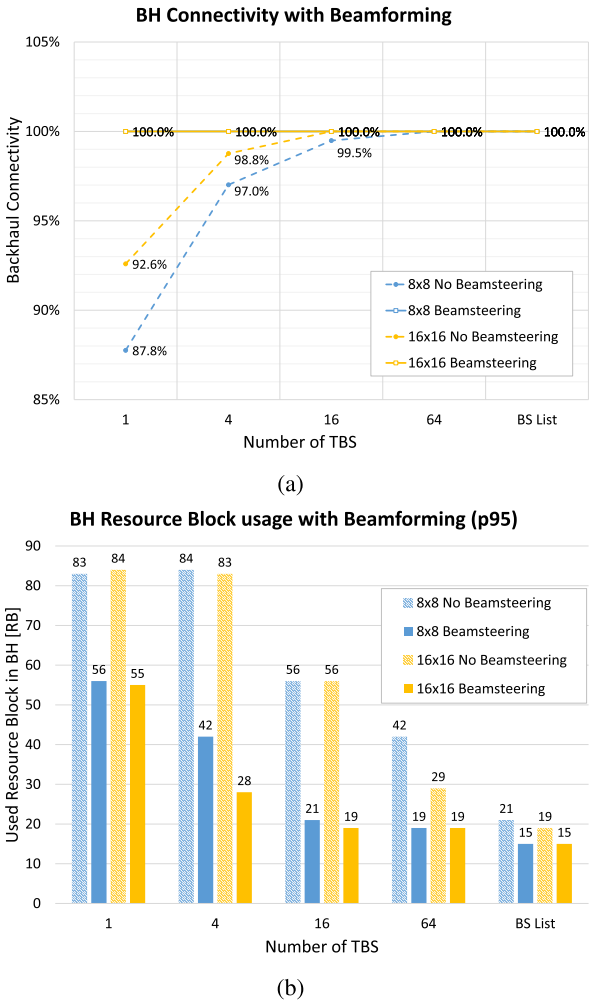

FIGURE 5. Scenario 1: BH performance a) BH Connectivity (p_{95}) compared with antenna size and available facilities for steering and no steering techniques. b) BH Resource Block usage (p_{95}).

from 36.8 Mbps (one TBS) up to 60.8 Mbps (operators TBS list) for 25 requested users.

5) SERVICE TIME

The average service time per carrier depends on the transmitted power of the UAV. For beam steering cases, the average service time is nearly 150 minutes (p_{95}) and will increment slightly depending on the availability of terrestrial infrastructure. For the cases of 16 TBS, 64 TBS and operator TBS list, the increment is 2%, 5% and 8% compared with the 1 and 4 TBS cases. However, three carriers are needed to support the whole event.

B. SCENARIO 2: MULTIBEAM BEAMFORMING IN THE BH NETWORK

In this second scenario, Multibeam beamforming in the BH network is evaluated. Here, we assume that the element gain of the MaMIMO antenna is the same in every sector. In contrast, the antenna transmission power is divided equally to each beam as described in (13).

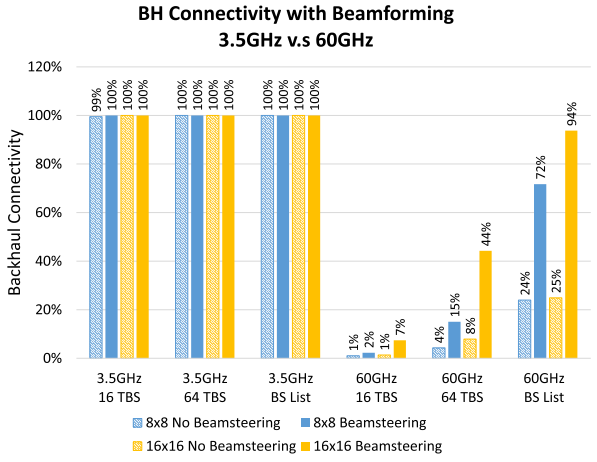

FIGURE 6. Scenario 1: Comparison of the performance of 3.5 GHz and 60 GHz in the BH link.

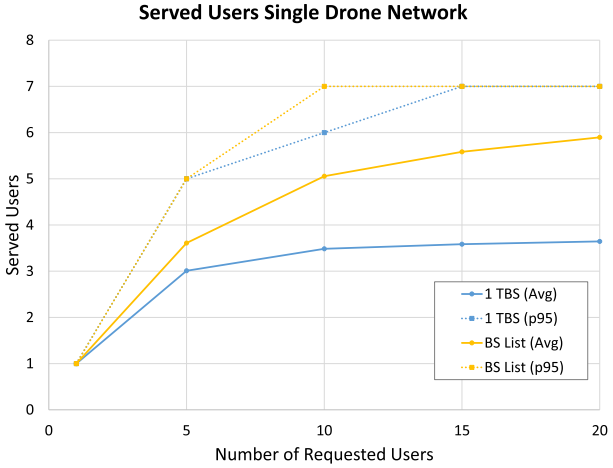

FIGURE 7. Scenario 1: Served capacity for single drone multi-user network.

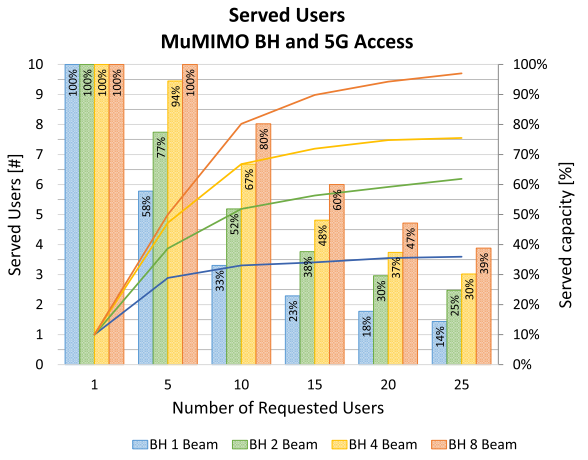

(a)

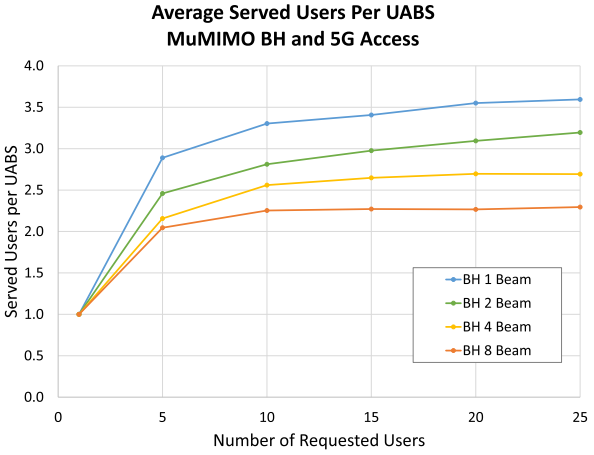

(b)

FIGURE 8. Scenario 2: Served capacity (p_{95}) for single drone multi-user network. a) Provided users. b) Served ground users per UABS.

We evaluate the performance of the maximum number of MIMO layers that expresses the maximum number of simultaneous beams over a MuMIMO antenna. In this case, we evaluate 1, 2, 4, and 8-layers; the latter was considered for future improvements of the UL, suitable for supporting 2 code words [61]. The following results are collected assuming the best performance case for the BH network, i.e., a 16 × 16 antenna system placed on the UABS to serve the ground users combined with the TBS allocation based on the operator BS list.

1) COVERAGE IN SCENARIO 2

Fig. 8a shows the provided user coverage (p_{95}) for the Multi-beam in the BH network. The lines represent the absolute number of served ground users while the boxes the percentage of served ground users. Blue, green, yellow, and orange represent the evaluated 1, 2, 4, and 8-layers, respectively. When Multi-beamforming is applied, the number of served ground users increases from 14% to 39% for 25 simultaneous ground users, as shown in the blue and orange boxes of Fig. 8a. Full coverage can only be provided to up to five ground users when using eight beams. One might expect ground users to be covered eight times more when using eight beams than one, but this is unfortunately not the case. This is because the number of served ground users per UABS is reduced when the number of beams increases from 3.6 users/UABS (blue line in Fig. 8b) down to 2.6 users/UABS (orange line in Fig. 8b). This is due to the division of the beam power in the BH that reduces the link's supported power, resulting in a limitation of the BH capacity per UABS. Furthermore, the capacity of the access network is a limiting factor here since the maximum bitrate for our narrow band 5G access network is 42 Mbps per UABS, so only each UABS can serve 4 ground users requesting 10 Mbps.

When using 1 and 2 beams, the number of UABSs that can be served simultaneously is the limiting factor: each beam can serve only 1 UABS. This is, however, no longer the case when increasing the number of supported beams to 4 and 8. In this case, the power per beam is the limiting factor:

3 and 4 UABSs could simultaneously be supported using 4 and 8 beams.

2) CAPACITY IN SCENARIO 2

The capacity served by the network increases more than 2.5 times when using eight beams compared to only1 beam, providing an average of 97 Mbps (p_{95}) for a 20 MHz channel, achieving a channel efficiency of 4.85 bit/s/Hz. This served capacity doubles the ones found [28] where the performance of the interference is considered. The BH resource block (RB) usage behaves comparably to the capacity: the number of used RBs is three times higher for eight beams than1 beam. Also, the number of RB per UABS is reduced by 2/3rds, consistent with the number of users per UABS in Fig. 8b.

C. SCENARIO 3: MULTIBEAM BEAMFORMING IN ACCESS AND BH NETWORKS

The third scenario considers the multibeam in both the access and BH network.

1) COVERAGE IN SCENARIO 3

Here, the number of served users increases significantly with the usage of multiuser beamforming in the access network. Fig. 9 shows that the p_{95} percentage of covered users (in boxes) rises from 32% to 69% when the number of access beams increases from 1 to 8 (blue and orange boxes) for 25 requested users. Compared to Scenario 2, only BH beamforming (see Sec V-B), more ground users can be covered, increasing the full coverage 100% from 5 to 10 users. Nonetheless, the behaviour of 4 access beams and access beams is very similar, with a small increment of less than 2%. This is because the power division for each beam reduces the maximum achievable power. This leads to the point where no more users could be served by the same UABS, maintaining the required SNR.

As a result, the number of served users per UABS is relatively constant, independent of the number of requested users. For 4 access beams, nearly 2.6 users/UABS are served, while almost 3.1 users/UABS are served for 8 access beams, a small increment of 20%.

The number of required UABSs to serve the ground users is reduced when the number of access beams increases. More users per UABS will be served when using more beams, reducing the need for more UABSs. In this case, only 5.5 drones (p_{95}) are needed for 8 access beams supporting 69% of the users, while 8 drones are necessary to support only 32% of the ground users with just one access beam. Here, the UABS requirements of 4 access beams and 8 access beams are similar, with a small increment of 10% for the 4 access beam case.

2) CAPACITY IN SCENARIO 3

The served capacity (p_{95}) of the network is presented in Fig. 9b. The requested capacity is described by the red dotted lines, whereas the straight lines represent the served capacity. For 4 and 8 access beams, the served capacity of 10 ground

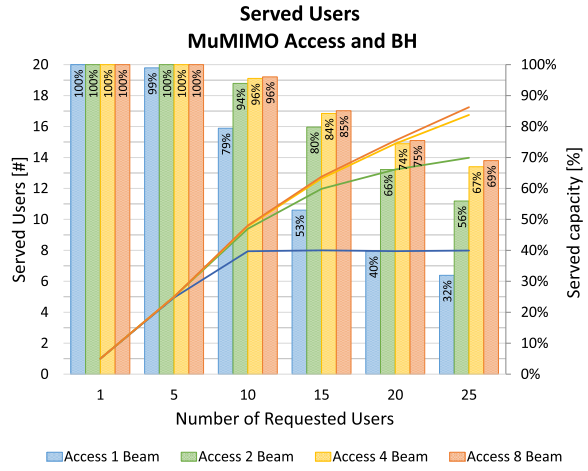

(a)

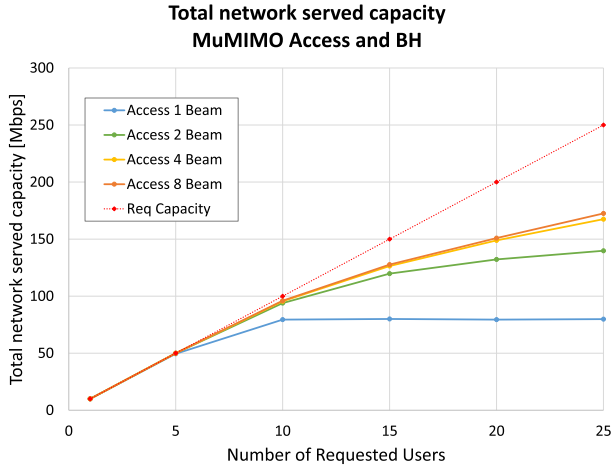

(b)

FIGURE 9. Scenario 3: Served users (p_{95}) in multibeam access and BH network. a) Served users b)Total served capacity for MuBF in access and BH.

users is covered. Unfortunately, the network capacity served by the UABSs is not sufficient to serve all the 25 requested users. This is because, for many access beams, the power per beam is reduced, reducing the SNR, which limits the served bitrate per beam. Here, up to 172 Mbps will be served with 20 MHz of BW in the BH and 32.4 Mbps per UABS with 5 MHz in the Access. This means an efficiency of 8.6 bit/sec/Hz in the BH network and 6.5 bit/sec/Hz in the access network. These results are comparable with the HBF technique found in [24] where efficiency of 8.6 bit/sec/Hz is found for nearly 25 dB of SNR, which is relatively higher than the experience in our simulations. Similarly, in [62], the usage of low complexity Electronically Steerable Parasitic Array Radiators (ESPARs) provide similar performance despite that the maximum antenna gain is nearly 17dB lower than our UPR, accounting 8 bit/sec/Hz with an SNR of 25dB for the BH link. This is achieved based on the antenna adaptation algorithm provided for the ESPARs.

TABLE 7. Key results for scenarios 2 and 3 with 25 ground users, 16 × 16 antenna size and BS list. p_{95} values shown.

Parameter	Units	Scenario 2 MuMIMO for only BH				Scenario 3 MuMIMO for Access and BH			
Access Beams		-	-	-	-	1	2	4	8
BH Beams		1	2	4	8	8	8	8	8
Coverage									
Served Users	%	14	25	30	39	32	56	67	69
Served Users/UABS	#	3.6	3.2	2.7	2.3	1	1.9	2.8	3.2
Used UABS	#	1.0	1.9	2.9	4.4	8.0	7.5	6.1	5.5
Capacity									
Network Capacity	Mbps	35.9	61.9	75.5	97.0	79.8	139.8	167.5	172.5
Capacity served/UABS	Mbps	35.9	31.9	26.9	22.9	10.0	18.8	27.8	32.4
Access Network eff	bit/s/Hz	7.2	6.4	5.8	4.6	2.0	3.8	5.6	6.5
BH Network eff	bit/s/Hz	1.8	3.2	3.8	4.9	4.0	7.0	8.8	8.6
BH RB usage	RB	50.4	86.9	107.4	144.0	133.1	226.0	266.0	256.6
BH RB usage/UABS	RB	50.4	44.9	38.2	33.7	16.7	30.4	44.2	48.0

In addition, the usage of the RB in the BH increases 2.7 times for 8 access beams compared with 1 beam, and a small increment in the bitrate per resource block is found in the 8 beam case, from 600 kbps/RB (1 beam) up to 672 kbps/RB (8 beams). This is because, for more traffic served in the access network, a more efficient allocation of the RB on the BH will be achieved, as explained in [34]. Besides, if fewer UABS are needed, the optimised network chooses UABS locations with better PL, allowing better MCS, and increasing the average bitrate per RB.

D. SUMMARY AND COMPARISON OF RESULTS

Finally, Table 7summarises the key results of the multiuser beamforming scenarios for a network using the BS list for the TBS locations, an antenna size 16 × 16, and 25 requested users. This Table collects the p_{95} results from the coverage and capacity perspective.

1) COVERAGE COMPARISON

The percentage of served users (p_{95}) increases from 14% in Scenario 2 up to 69% in the best case of Scenario 3. However, this is not sufficient to serve all the requested users. The average number of served users per UABS is limited: around 3 users/UABS (3.2 for the best-case scenario), 40% of the maximum theoretical users per UABS (8 users). The required number of UABS behaves opposite for Scenario 2 compared with Scenario 3. For Scenario 2, the used UABS rises if the number of beams increases since BH beams are directly related to the number of UABS. While for Scenario 3, the more access beams available, the fewer UABS are needed to support the same number of requested ground users.

2) CAPACITY COMPARISON

The performance of the capacity is significantly better for Scenario 3. Here, the best-case supports up to 172.5 Mbps (p_{95}) compared with only 97.0 Mbps of Scenario 2. Similarly, the resource block usage is much higher in Scenario 3 with up to 256 RB and only 144 RB for Scenario 2. The RB per UABS is also 42% larger for scenario 2. The channel efficiency also improves in Scenario 3, having a maximum of 6.5 bit/s/Hz for the access network and 8.6 bit/s/Hz for the BH network, compared with the 4.6 bit/s/Hz and 4.9 bit/s/Hz for scenario 2.

VI. CONCLUSION AND FUTURE WORK

Unmanned Aerial Base Stations are a promising solution for fast deployable networks in crowded scenarios or when terrestrial connectivity is limited. As the drones' technologies provide longer flying times, coverage of UABS could be extended. This imposes a challenge to the BH link where the restriction of the propagation losses limits the link range. To surpass this, digital beamforming will increase the antenna gain and improve the access and BH link quality.

This work evaluates the digital beamforming technique's performance to support MuMIMO in the BH and the access networks. To this end, we implement a simulation tool that includes beamforming capabilities in a mobile scenario for an UABS-aided network in a realistic environment. Simulation results show that using the actual terrestrial BS locations improves the connectivity performance compared with a private network. If the beamsteering technique is used in the BH, the served capacity increases two times. Moreover, when MuMIMO is used, we found that the user coverage increases four times compared to a single beam MIMO network. For the proposed scenario, we achieved a channel efficiency of 6.5 bit/s/Hz for the access link and 8.5 bit/s/Hz for the BH link, comparable with results found in the literature.

Future work will cover a dynamic ground facility location that can extend the range of the BH link and will enable improved user coverage. It will include an upgrade on the sensibility of recent 5G New Radio (5GNR) transceivers to improve the requested SNR of the system for the 3.5 GHz, 26 GHz, and 60 GHz bands. Finally, we will complement our work by modelling and evaluating beam tracking techniques to maintain beam alignment in terms of the physical layer and drone movement. We will develop a channel model to include the impact of velocity on the capacity and performance of the system.

REFERENCES

[1] Y. Kawamoto, H. Nishiyama, N. Kato, F. Ono, and R. Miura, "Toward future unmanned aerial vehicle networks: Architecture, resource allocation and field experiments," *IEEE Wireless Commun.*, vol. 26, no. 1, pp. 94–99, Feb. 2019.

[2] M. Mozaffari, W. Saad, M. Bennis, Y.-H. Nam, and M. Debbah, "A tutorial on UAVs for wireless networks: Applications, challenges, and open problems," *IEEE Commun. Surveys Tuts.*, vol. 21, no. 3, pp. 2334–2360, 3rd Quart., 2019.

[3] B. Alzahrani, O. S. Oubbati, A. Barnawi, M. Atiquzzaman, and D. Alghazzawi, "UAV assistance paradigm: State-of-the-art in applications and challenges," *J. Netw. Comput. Appl.*, vol. 166, Sep. 2020, Art. no. 102706. [Online]. Available: https://www.sciencedirect.com/science/article/pii/S1084804520301806

[4] M. Mozaffari, W. Saad, M. Bennis, and M. Debbah, "Efficient deployment of multiple unmanned aerial vehicles for optimal wireless coverage," *IEEE Commun. Lett.*, vol. 20, no. 8, pp. 1647–1650, Aug. 2016.

[5] A. Colpaert, E. Vinogradov, and S. Pollin, "Aerial coverage analysis of cellular systems at LTE and mmWave frequencies using 3D city models," *Sensors*, vol. 18, no. 12, p. 4311, Dec. 2018. [Online]. Available: https://www.mdpi.com/1424-8220/18/12/4311

[6] S. De Bast, E. Vinogradov, and S. Pollin, "Cellular coverage-aware path planning for UAVs," in *Proc. IEEE 20th Int. Workshop Signal Process. Adv. Wireless Commun. (SPAWC)*, Jul. 2019, pp. 1–5.

[7] A. Colpaert, E. Vinogradov, and S. Pollin, "3D beamforming and handover analysis for UAV networks," in *Proc. IEEE Globecom Workshops (GC Wkshps*, Dec. 2020, pp. 1–6.

[8] A. Colpaert, M. Raes, E. Vinogradov, and S. Pollin, "Drone delivery: Reliable cellular UAV communication using multi-operator diversity," in *Proc. IEEE Int. Conf. Commun. (ICC)*, Feb. 2022, pp. 1–6.

[9] T. L. Marzetta, E. G. Larsson, H. Yang, and H. Q. Ngo, *Fundamentals of Massive MIMO*. Cambridge, U.K.: Cambridge Univ. Press, 2016. [Online]. Available: https://www.cambridge.org/core/books/fundamentals-of-massive-mimo/C43AF993A6DA7075EC5F186F6BAC914B

[10] P. Chandhar, D. Danev, and E. Larsson, "Massive MIMO for communications with drone swarms," *IEEE Trans. Wireless Commun.*, vol. 17, no. 3, pp. 1604–1629, Mar. 2018.

[11] H. He, S. Zhang, Y. Zeng, and R. Zhang, "Joint altitude and beamwidth optimization for UAV-enabled multiuser communications," *IEEE Commun. Lett.*, vol. 22, no. 2, pp. 344–347, Feb. 2018.

[12] G. Geraci, A. G. Rodriguez, L. G. Giordano, D. L. Pérez, and E. Björnson, "Understanding UAV cellular communications: From existing networks to massive MIMO," *IEEE Access*, vol. 6, pp. 67853–67865, 2018.

[13] A. Garcia-Rodriguez, G. Geraci, D. Lopez-Perezp, L. G. Giordano, M. Ding, and E. Bjornson, "The essential guide to realizing 5G-connected UAVs with massive MIMO," *IEEE Commun. Mag.*, vol. 57, no. 12, pp. 84–90, Oct. 2019.

[14] L. Zhang, H. Zhao, S. Hou, Z. Zhao, H. Xu, X. Wu, Q. Wu, and R. Zhang, "A survey on 5G millimeter wave communications for UAV-assisted wireless networks," *IEEE Access*, vol. 7, pp. 117460–117504, 2019.

[15] L. Liu, S. Zhang, and R. Zhang, "Multi-beam UAV communication in cellular uplink: Cooperative interference cancellation and sum-rate maximization," *IEEE Trans. Wireless Commun.*, vol. 18, no. 10, pp. 4679–4691, Oct. 2019.

[16] A. Fouda, A. S. Ibrahim, I. Guvenc, and M. Ghosh, "Interference management in UAV-assisted integrated access and backhaul cellular networks," *IEEE Access*, vol. 7, pp. 104553–104566, 2019.

[17] N. Tafintsev, M. Valkama, D. Moltchanov, M. Gerasimenko, M. Gapeyenko, J. Zhu, S.-P. Yeh, N. Himayat, S. Andreev, and Y. Koucheryavy, "Aerial access and backhaul in mmWave B5G systems: Performance dynamics and optimization," *IEEE Commun. Mag.*, vol. 58, no. 2, pp. 93–99, Feb. 2020.

[18] G. Castellanos, M. Deruyck, L. Martens, and W. Joseph, "Performance evaluation of direct-link backhaul for UAV-aided emergency networks," *Sensors*, vol. 19, no. 15, p. 3342, Jul. 2019. [Online]. Available: https://www.mdpi.com/1424-8220/19/15/3342

[19] B. Halvarsson, K. Larsson, M. Thurfjell, K. Hiltunen, K. Tran, P. Machado, D. Juchnevicius, and H. Asplund, "5G NR coverage, performance and beam management demonstrated in an outdoor urban environment at 28 GHz," in *Proc. IEEE 5G World Forum (5GWF)*, Jul. 2018, pp. 416–421.

[20] E. Vinogradov, H. Sallouha, S. De Bast, M. Azari, and S. Pollin, "Tutorial on UAVs: A blue sky view on wireless communication," *J. Mobile Multimedia*, vol. 14, no. 4, pp. 395–468, 2018.

[21] M. Mozaffari, A. T. Z. Kasgari, W. Saad, M. Bennis, and M. Debbah, "Beyond 5G with UAVs: Foundations of a 3D wireless cellular network," *IEEE Trans. Wireless Commun.*, vol. 18, no. 1, pp. 357–372, Jan. 2019.

[22] X. Lin, V. Yajnanarayana, S. D. Muruganathan, S. Gao, H. Asplund, H. Maattanen, M. Bergstrom, S. Euler, and Y.-E. Wang, "The sky is not the limit: LTE for unmanned aerial vehicles," *IEEE Commun. Mag.*, vol. 56, no. 4, pp. 204–210, Apr. 2018.

[23] M. Mozaffari, W. Saad, M. Bennis, and M. Debbah, "Communications and control for wireless drone-based antenna array," *IEEE Trans. Commun.*, vol. 67, no. 1, pp. 820–834, Jan. 2019.

[24] Z. Xiao, L. Zhu, and X.-G. Xia, "UAV communications with millimeter-wave beamforming: Potentials, scenarios, and challenges," *China Commun.*, vol. 17, no. 9, pp. 147–166, Sep. 2020.

[25] Z. Xiao, P. Xia, and X.-G. Xia, "Enabling UAV cellular with millimeter-wave communication: Potentials and approaches," *IEEE Commun. Mag.*, vol. 54, no. 5, pp. 66–73, May 2016.

[26] Y. Huang, Q. Wu, T. Wang, G. Zhou, and R. Zhang, "3D beam tracking for cellular-connected UAV," *IEEE Wireless Commun. Lett.*, vol. 9, no. 5, pp. 736–740, May 2020.

[27] W. Zhong, L. Xu, Q. Zhu, X. Chen, and J. Zhou, "MmWave beamforming for UAV communications with unstable beam pointing," *China Commun.*, vol. 16, no. 1, pp. 37–46, Jan. 2019.

[28] T. Izydorczyk, G. Berardinelli, P. Mogensen, M. M. Ginard, J. Wigard, and I. Z. Kovacs, "Achieving high UAV uplink throughput by using beamforming on board," *IEEE Access*, vol. 8, pp. 82528–82538, 2020.

[29] Y. Huang, Q. Wu, R. Lu, X. Peng, and R. Zhang, "Massive MIMO for cellular-connected UAV: Challenges and promising solutions," *IEEE Commun. Mag.*, vol. 59, no. 2, pp. 84–90, Feb. 2021.

[30] L. Wang, Y. L. Che, J. Long, L. Duan, and K. Wu, "Multiple access mmWave design for UAV-aided 5G communications," *IEEE Wireless Commun.*, vol. 26, no. 1, pp. 64–71, Feb. 2019.

[31] B. Halvarsson, A. Simonsson, A. Elgcrona, R. Chana, P. Machado, and H. Asplund, "5G NR testbed 3.5 GHz coverage results," in *Proc. IEEE 87th Veh. Technol. Conf. (VTC Spring)*, Jun. 2018, pp. 1–5.

[32] A. Fouda, A. S. Ibrahim, I. Güvenç, and M. Ghosh, "UAV-based in-band integrated access and backhaul for 5G communications," in *Proc. IEEE 88th Veh. Technol. Conf. (VTC-Fall)*, Aug. 2018, pp. 1–5.

[33] M. Deruyck, J. Wyckmans, W. Joseph, and L. Martens, "Designing UAV-aided emergency networks for large-scale disaster scenarios," *EURASIP J. Wireless Commun. Netw.*, vol. 2018, no. 1, pp. 1–12, Dec. 2018. [Online]. Available: https://jwcn-eurasipjournals.springeropen.com/articles/10.1186/s13638-018-1091-8

[34] G. Castellanos, M. Deruyck, L. Martens, and W. Joseph, "Multi-frequency backhaul analysis for UABS in disaster situations," in *Proc. Int. Conf. Wireless Mobile Comput., Netw. Commun. (WiMob)*, Oct. 2019, pp. 221–225.

[35] A. F. Molisch, V. V. Ratnam, S. Han, Z. Li, S. L. H. Nguyen, L. Li, and K. Haneda, "Hybrid beamforming for massive MIMO: A survey," *IEEE Commun. Mag.*, vol. 55, no. 9, pp. 134–141, Sep. 2017.

[36] N. Jindal, "MIMO broadcast channels with finite-rate feedback," *IEEE Trans. Inf. Theory*, vol. 52, no. 11, pp. 5045–5060, Nov. 2006.

[37] E. Bala, K. J.-L. Pan, R. Olesen, and D. Grieco, "Zero-forcing beamforming codebook design for MU-MIMO OFDM systems," in *Proc. IEEE 68th Veh. Technol. Conf.*, Sep. 2008, pp. 1–5.

[38] T. Younas, J. Li, J. Arshad, H. M. Munir, M. M. Tulu, and O. Younas, "Performance of ZF and RZF in massive MIMO with channel aging," in *Proc. 3rd IEEE Int. Conf. Comput. Commun. (ICCC)*, Dec. 2017, pp. 930–934.

[39] T. A. Sheikh, J. Bora, and M. A. Hussain, "Capacity maximizing in massive MIMO with linear precoding for SSF and LSF channel with perfect CSI," *Digit. Commun. Netw.*, vol. 7, no. 1, pp. 92–99, Feb. 2021. [Online]. Available: https://www.sciencedirect.com/science/article/pii/S2352864819300343

[40] X. Gao, L. Dai, Z. Gao, T. Xie, and Z. Wang, "Precoding for mmWave massive MIMO," in *mmWave Massive MIMO*, S. Mumtaz, J. Rodriguez, and L. Dai, Eds. New York, NY, USA: Academic, Jan. 2017, ch. 5, pp. 79–111. [Online]. Available: https://www.sciencedirect.com/science/article/pii/B9780128044186000054

[41] C.-S. Wu, C.-H. Chen, C.-R. Tsai, and A.-Y. Wu, "Joint RF/baseband grouping-based codebook design for hybrid beamforming in mmWave MIMO systems," in *Proc. IEEE Int. Conf. Signal Process., Commun. Comput. (ICSPCC)*, Aug. 2016, pp. 1–6.

[42] H. Seleem, A. I. Sulyman, and A. Alsanie, "Hybrid precoding-beamforming design with Hadamard RF codebook for mmWave large-scale MIMO systems," *IEEE Access*, vol. 5, pp. 6813–6823, 2017.

[43] S. Hanna, E. Krijestorac, and D. Cabric, "UAV swarm position optimization for high capacity MIMO backhaul," *IEEE J. Sel. Areas Commun.*, vol. 39, no. 10, pp. 3006–3021, Oct. 2021.

[44] *5G; Study on Channel Model for Frequencies From 0.5 to 100 GHz (3GPP TR 38.901 Version 15.0.0 Release 15)*, document ETSI TR 138 901 V15.0.0, ETSI, Jul. 2018.

[45] C. Balanis, *Antenna Theory: Analysis and Design*, 3rd ed. Hoboken, NJ, USA: Wiley, 2005.

[46] H. Chang, C.-X. Wang, Y. He, Z. Bai, J. Sun, and W. Zhang, "Multi-user UAV channel modeling with massive MIMO configuration," in *Proc. IEEE 94th Veh. Technol. Conf. (VTC-Fall)*, Sep. 2021, pp. 01–06.

[47] S. Gunnarsson, J. Flordelis, L. Van Der Perre, and F. Tufvesson, "Channel hardening in massive MIMO: Model parameters and experimental assessment," *IEEE Open J. Commun. Soc.*, vol. 1, pp. 501–512, 2020.

[48] J. Zhao, F. Gao, Q. Wu, S. Jin, Y. Wu, and W. Jia, "Beam tracking for UAV mounted SatCom on-the-move with massive antenna array," *IEEE J. Sel. Areas Commun.*, vol. 36, no. 2, pp. 363–375, Feb. 2018.

[49] J. R. Reis, A. Hammoudeh, N. Copner, T. Fernandes, and R. F. S. Caldeirinha, "2D agile beamsteering using an electronically reconfigurable transmitarray," in *Proc. 13th Eur. Conf. Antennas Propag. (EuCAP)*, 2019, pp. 1–5.

[50] E. Chu, J. Yoon, and B. Jung, "A novel link-to-system mapping technique based on machine learning for 5G/IoT wireless networks," *Sensors*, vol. 19, no. 5, p. 1196, Mar. 2019. [Online]. Available: https://www.mdpi.com/1424-8220/19/5/1196

[51] *Technical Specification Group Radio Access Network; NR; User Equipment (UE) Radio Access Capabilities (Release 15)*, document TS 38.306 V15.12.0, 3GPP, Valbonne, France, Dec. 2020.

[52] U. Siddique, H. Tabassum, E. Hossain, and D. I. Kim, "Wireless backhauling of 5G small cells: Challenges and solution approaches," *IEEE Wireless Commun.*, vol. 22, no. 5, pp. 22–31, Oct. 2015. [Online]. Available: http://ieeexplore.ieee.org/document/7306534/

[53] *Considerations for the 3.5 GHz IMT Range: Getting Ready for Use*, GSMA, London, U.K., May 2017.

[54] M. J. Jiao, "5G challenges and spectrum plan," Huawei Technol., Bogota, Colombia., Tech. Rep. 001/2016, 2016.

[55] *Technical Specification Group Radio Access Network; Study on Enhanced LTE Support for Aerial Vehicles (Release 15)*, document TR 36.777, 3GPP, Valbonne, France, 2017.

[56] A. Al-Hourani, S. Kandeepan, and A. Jamalipour, "Modeling air-to-ground path loss for low altitude platforms in urban environments," in *Proc. IEEE Global Commun. Conf. (GLOBECOM)*, Dec. 2014, pp. 2898–2904.

[57] M. Matalatala Tamasala, S. Shikhantsov, M. Deruyck, E. Tanghe, D. Plets, S. K. Goudos, L. Martens, and W. Joseph, "Combined ray-tracing/FDTD and network planner methods for the design of massive MIMO networks," *IEEE Access*, vol. 8, pp. 206371–206387, 2020.

[58] *Harris Aerial H4 Hybrid Drone*. Accessed: Dec. 20, 2021. [Online]. Available: https://www.harrisaerial.com/carrier-h4-hybrid-drone/

[59] M. Deruyck, E. Tanghe, W. Joseph, W. Vereecken, M. Pickavet, B. Dhoedt, and L. Martens, "Towards a deployment tool for wireless access networks with minimal power consumption," in *Proc. IEEE 21st Int. Symp. Pers., Indoor Mobile Radio Commun. Workshops*, Sep. 2010, pp. 295–300. [Online]. Available: http://ieeexplore.ieee.org/document/5670382/

[60] G. Castellanos, M. Deruyck, L. Martens, and W. Joseph, "System assessment of WUSN using NB-IoT UAV-aided networks in potato crops," *IEEE Access*, vol. 8, pp. 56823–56836, 2020.

[61] *Technical Specification Group Services and System Aspects; Release 15 Description; Summary of Rel-15 Work Items (Release 15)*, document TR 21.915 V15.0.0, 3GPP, Valbonne, France, Sep. 2019.

[62] K. Maliatsos, P. S. Bithas, and A. G. Kanatas, "A low-complexity reconfigurable multi-antenna technique for non-terrestrial networks," *Frontiers Commun. Netw.*, vol. 2, pp. 1–16, Jun. 2021. [Online]. Available: https://www.frontiersin.org/article/10.3389/frcmn.2021.696111

GERMAN CASTELLANOS was born in Bogota, Colombia, in June 1981. He received the B.Sc. degree in electronics engineering from the Colombian School of Engineering, Bogota, in 2004, and the Master of Philosophy degree in computer engineering from The University of Newcastle, Australia, in 2012. He is currently pursuing the Ph.D. degree in electrical engineering with Ghent University, Ghent, Belgium, with IMEC–WAVES Research Group. Since 2005, he has been a Researcher at the Colombian School of Engineering. His research interests include new radio access networks for mobile systems and the coexistence between wireless services.

ACHIEL COLPAERT received the B.Sc. and M.Sc. degrees in electrical engineering from KU Leuven, Belgium, in 2015 and 2017, respectively, where he is currently pursuing the Ph.D. degree, focusing on high-throughput wireless links for UAV applications. His main research interests include mmWave and outdoor wireless modeling.

MARGOT DERUYCK (Member, IEEE) was born in Kortrijk, Belgium, in July 1985. She received the M.Sc. degree in computer science engineering and the Ph.D. degree from Ghent University, Ghent, Belgium, in 2009 and 2015, respectively. From September 2009 to January 2015, she was a Research Assistant with the Department of Information Technology, IMEC–Wireless, Acoustics, Environment and Expert Systems (WAVES), Ghent University. Her scientific work is focused on green wireless access networks with minimal power consumption and minimal exposure from human beings. This work led to her Ph.D. degree. Since January 2015, she has been a Postdoctoral Researcher at Ghent University, where she currently continues her work in the green wireless access networks. She is a Postdoctoral Fellow of the Research Foundation Flanders (FWO-V).

EMMERIC TANGHE was born in Tielt, Belgium, in August 1982. He received the M.Sc. and Ph.D. degrees in electrical engineering from Ghent University, Ghent, Belgium, in 2005 and 2011, respectively. From September 2005 to May 2011, he was a Research Assistant with the Department of Information Technology, Ghent University (IMEC-UGent/INTEC). Since May 2011, he has been a Postdoctoral Researcher with Ghent University and currently continues his work in propagation modeling. From October 2012 to September 2018, he was a Postdoctoral Fellow of the Research Foundation Flanders (FWO-V). In October 2015, he became a part-time Professor in medical applications of electromagnetic fields in and around the human body. His scientific work focused on modeling indoor and outdoor propagation through field measurements.

EVGENII VINOGRADOV received the Diploma degree in engineering from Saint-Petersburg Electrotechnical University, Russia, and the Ph.D. degree from UCLouvain, Belgium. His doctoral research was focused on multidimensional stochastic channel modeling. He is currently an Associate Researcher with the KU Leuven's Electrical Engineering Department. His research interests include 6G technologies as non-terrestrial and cell-free networks.

LUC MARTENS (Member, IEEE) received the M.Sc. degree in electrical engineering from Ghent University, Ghent, Belgium, in 1986, and the Ph.D. degree, in 1990. From 1986 to 1990, he was a Research Assistant with the Department of Information Technology, Ghent University. During this period, his scientific research focused on the physical aspects of hyperthermic cancer therapy. His research dealt with electromagnetic and thermal modeling and the development of measurement systems for that application. Since 1991, he has been managing the WAVES Research Group, INTEC. The WAVES Research Group has been a part of the IMEC Institute, since 2004. Since 1993, he has been a Professor at Ghent University.

SOFIE POLLIN received the Ph.D. degree (Hons.) from KU Leuven, in 2006. From 2006 to 2008, she continued her research on wireless communications, energy-efficient networks, cross-layer design, coexistence, and cognitive radio at UC Berkeley. In 2008, she returned to IMEC to become a Principal Scientist at the Green Radio Team. She is currently an Associate Professor with the Electrical Engineering Department, KU Leuven. Her research interests include networked systems that require ever more dense, heterogeneous, battery-powered, and spectrum constrained networks. She is a BAEF Fellow and a Marie Curie Fellow.

WOUT JOSEPH (Senior Member, IEEE) was born in Ostend, Belgium, in October 1977. He received the M.Sc. degree in electrical engineering from Ghent University, Belgium, in July 2000. From September 2000 to March 2005, he was a Research Assistant at the Ghent University's Department of Information Technology (INTEC). During this period, his scientific work was focused on electromagnetic exposure assessment. His research work dealt with measuring and modeling electromagnetic fields around base stations for mobile communications related to the health effects of exposure to electromagnetic radiation. This work led to his Ph.D. degree, in March 2005. Since April 2005, he has been a Postdoctoral Researcher at IBBT-Ugent/Interdisciplinary Institute for Broadband Technology (INTEC). Since October 2007, he has been a Postdoctoral Fellow of the Research Foundation Flanders (FWO-V). Since October 2009, he has been a Professor in experimental characterization of wireless communication systems. His professional interests include electromagnetic field exposure assessment, propagation for wireless communication systems, antennas, and calibration. Furthermore, he specializes in wireless performance analysis and quality of experience.